Available on CMS information server

CMS NOTE 2008/027

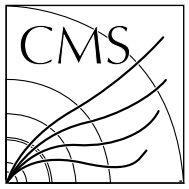

The Compact Muon Solenoid Experiment

CMS Note

Mailing address: CMS CERN, CH-1211 GENEVA 23, Switzerland

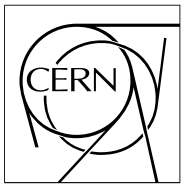

October 8, 2008

First Measurements of the Performance of the Barrel RPC System in CMS

A. Colaleo, F. Loddo, M. Maggi, A. Ranieri

INFN Sezione di Bari, Italy

M. Abbrescia, G. Iaselli, B. Marangelli, S. Natali, S. Nuzzo, G. Pugliese, F. Romano, G. Roselli, R. Trentadue, S. Tupputi

Dipartimento Interateneo di Fisica and Sezione INFN, Bari, Italy

P. Baesso, A. Grelli, M. Necchi, D. Pagano, S.P. Ratti, P. Vitulo, C. Viviani

Dipartimento di Fisica Nucleare e Teorica and Sezione INFN, Pavia, Italy

P. Paolucci, D. Piccolo

INFN, Sezione di Napoli, Italy

A. Cimmino, D. Lomidze, P. Noli

Dipartimento di Fisica e Sezione INFN, Napoli, Italy

L. Benussi, M. Bertani, S. Bianco, D. Colonna[a)b)], F.L. Fabbri

INFN Laboratori Nazionali di Frascati, Italy

A. Dimitrov, L. Litov, B. Pavlov, P. Petkov

Faculty of Physics Sofia University, Bulgaria

T. Anguelov, V. Genchev, P. Iaydjiev, B. Panev, S. Stoykova, G. Sultanov, R. Trayanov

INRNE, Bulgarian Academy of Sciences, Bulgaria

R. Guida, I. Segoni

CERN, Geneva, Switzerland

C.A. Carrillo Montoya

Universidad de Los Andes, Bogota, Colombia

G. Polese, T. Tuuva

Lappeenranta Univ. of Technology, Finland

K. Bunkowski, M. Cwiok, K. Doroba, A. Kalinowski, M. Konecki, J. Krolikowski, K. Kierzkowski, I.M. Kudla, W. Oklinski, M. Pietrusinski

Institute of Experimental Physics, University of Warsaw, Warsaw, Poland

M. Bluj, T. Fruboes, M. Gorski, R. Gokieli, M. Kazana, M. Szleper, G. Wrochna, P. Zalewski

Soltan Institute for Nuclear Studies, Warsaw, Poland

K.T. Pozniak, W. Zabolotny

Institute of Electronics Systems, Warsaw University of Technology, Warsaw, Poland

W. Whitaker

California State University, Fresno, USA

Abstract

During the summer 2006, a first integrated test of a part of the CMS experiment was performed at CERN collecting a data sample of several millions of cosmic rays events. A fraction of the Resistive Plate Chambers system was successfully operated. Results on the RPC performance are reported.

[a] also at CERN, Geneva, Switzerland

[b] also at Facoltá Ingegneria Universitá di Roma “La Sapienza”, Italy

1 Introduction

The Compact Muon Solenoid (CMS) [1, 2] experiment at the Large Hadron Collder (LHC) is based on high magnetic field (4 T), which with the fine read-out granularity of the detector trigger system will allow a preliminary transverse momentum assignment of muons [3]. The bunch crossing (BX) of the proton beams has been designed to be 25 ns to achieve high luminosity. A fast timing trigger detector is, therefore, required to properly determine the BX assignment of the muon candidates. CMS is equipped with a redundant Muon system based on Drift Tube chambers (DT) and Cathode Strip Chambers (CSC) respectively in the barrel and endcap regions for precise position measurement; in addition, Resistive Plate Chambers (RPC) are used for bunch crossing identification. The RPC trigger system is one of the largest ever built detector employing this technology [2].

In summer 2006, for the first time, the CMS detector was closed and the super conducting magnet was ramped up to its nominal value for commissioning and field map measurements. During this test, named Magnetic Test and Cosmic Challenge (MTCC), a portion of the Muon and the calorimeter systems was operated under cosmic rays to study the global CMS behavior by combining information from different sub-detectors. Advanced version of the final read-out, data acquisition and control system protocols were employed. The main goals for the RPC system were the determination of the synchronization and operation procedures, the assessment of the trigger capability and the study of the chambers' performance.

This paper reports only results on the performance of the RPC barrel system. Additional information on the global behavior of CMS can be found in [4].

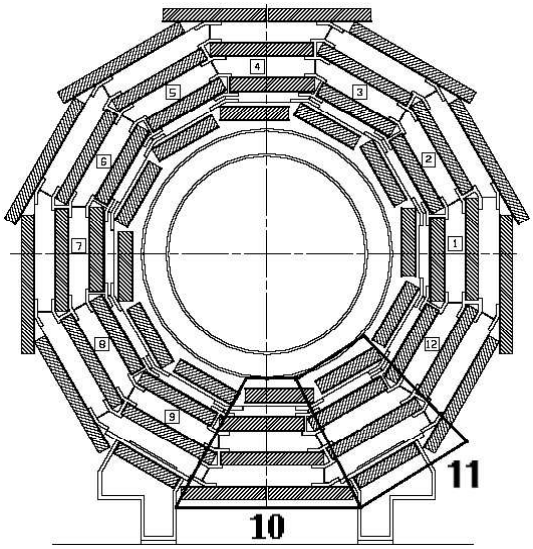

Figure 1: An (r, ϕ) schematic view of wheel W_{+2}, the sectors under test are highlighted.

2 Experimental set-up

In the barrel iron yoke, the RPC muon chambers form six coaxial sensitive cylinders around the beam axis approximated with concentric dodecagon arrays and subdivided into five wheels composed by 12 sectors. The sectors of each wheel cover a region of 30^o in ϕ and about 0.1 in pseudorapidity η with projective read-out geometry with respect to the interaction point. The wheels are denoted, hereafter, by the notation W_i where i is in the -2, 2 range and the relative sector number runs from 1 to 12. Each sector of a wheel comprises six layers of RPC chambers. Two layers are in the first and second Muon station above (Inner) and below (Outer) the DT Chamber. The third and fourth Muon stations are equiped only with the Inner layer that is covered by two RPC muon chambers apart for sector 4 and 10, where the fourth stations comprises two DT chambers each with one (sector 4) or two (sector 10) RPC chambers, and sector 9 and 11, where there is only one RPC muon chamber. A more detailed geometrical description of the detector can be found in [5].

Each chamber is read-out by electrode strips running along the beam-axis direction to measure the transverse momentum of the muon particles. The strip width varies from 2.3 cm for the inner layer to 4.1 cm for outer layer. To improve the time resolution the strips are divided into two or three parts called η-partitions. During the MTCC, three bottom sectors, sector 10 and 11 belonging to W_{+2} and sector 10 of W_{+1}, were operated. In Fig. 1 a (r, ϕ)

schematic view of wheel W_{+2} is shown with the sectors under test highlighted.

The 23 chambers, representing 5% of the entire Barrel RPC system, were all operated at a nominal voltage of 9.2 kV. The chambers reached, in this conditions, 90% efficiency or higher. Most of the results are given in terms of the effective operating voltage, HV_{eff}, which is obtained from the nominal values after pressure and temperature corrections, to account for their variations during the running period [6]. On average HV_{eff} was about 9.6 kV. The CMS RPC standard gas mixture, i.e. 96.2% $C_2H_2F_4$, 3.5% i-C_4H_{10}, 0.3% SF_6, was used.

The strip signals were discriminated and shaped into 100 ns logic pulses by the front-end boards [7] with 220 mV threshold, corresponding to a minimum signal charge of about 120 fC. All signals are propagated to the Link Boards (LB) placed on the detector periphery. The LBs synchronize the signals to the 40 MHz clock and, after data compression, send them to the Trigger Boards located in the control room, where the trigger algorithm based on pattern recognition is performed by Pattern Comparator (PAC) devices [8]. The Trigger Boards are part of the readout chain and data were also collected via their control system.

The PAC algorithm has been specifically developed to identify muon tracks coming from the interaction point. It is therefore not fully adequate for atmospheric muons, although some provisional modification of the algorithm for the sectors under operation made possible its application for the MTCC. In addition, in view of detector commissioning and maintenance during the LHC shutdown periods, the development of a special RPC trigger for cosmic ray muons has been foreseen: the RPC Balcony Collector (RBC) that was implemented in the system and used as a main trigger signal. The RBC receives from the LB the OR signal of each eta-partition. The trigger logic is based on pattern comparator with a preloaded pattern set and produces a sector-based cosmic trigger with a selectable majority level from 1/6 to 6/6. It has, in addition, several features such as: masking and forcing capability of the eta-partitions to increase the trigger selectivity on specific patterns and extra latency configuration for synchronization purposes. More details on the RBC trigger electronics can be found in [9]. During the MTCC, the DT system was providing the trigger. This was exploited for an unbiased study of the RPC system.

A sample of about twenty million events was collected with different trigger and operating conditions.

3 Experimental methods

The interplay between the RPC and DT system allows the determination of the timing of the trigger system and establish local reconstruction for fast determination of the RPC performance.

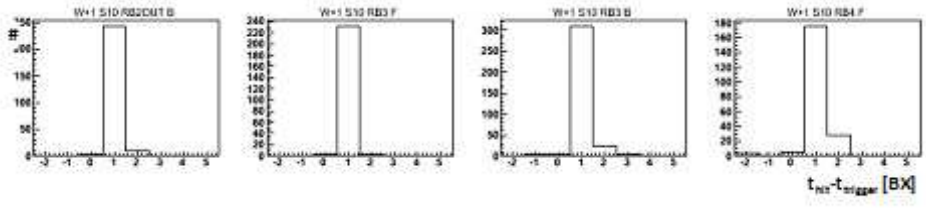

Figure 2: Distributions of the chamber hits BX with respect to the trigger time. BX number equal to 1 corresponds to the trigger signal.

At the LHC the crossings of beam bunches occur every 25 ns. The muons which originate from the proton-proton collisions are produced with very narrow timing (the time of bunches overlap is about 1 ns). However, the chamber hits are spread in time as the result of several effects like the difference of muon track lengths with different bending and the signal propagation along the strips, and others [10]. Moreover, the total timing of the signals received by the LBs varies among them, since the chambers have different distances to the interaction point and the cables connecting the chambers with the LBs also have different lengths. The asynchronous signals from chambers are assigned to the proper clock period by the Synchronization Unit of the LBs.A time window is set such that all muon hits, originating from the same bunch crossing, are assigned to the proper clock period [11]. An initial window position is calculated on the basis of the muons time of flight and the length of the signal cables. A subsequent analysis of the initial collected data allows the refinement of the time window position. In case of the cosmic muons (distributed randomly in time) the position of the windows can be defined with arbitrary offset (the same for all LBs). The distributions of the chamber hits BX with respect to the trigger time is presented in Fig. 2. BX number equal to 1 corresponds to the trigger signal. By changing the value of offset, the RPC trigger can also be aligned with the trigger provided by the Drift Tube system. The difference between the two reception times, before

and after the correction, is shown respectively in Fig 3a and 3b. Only the events where both systems produced the trigger are included.

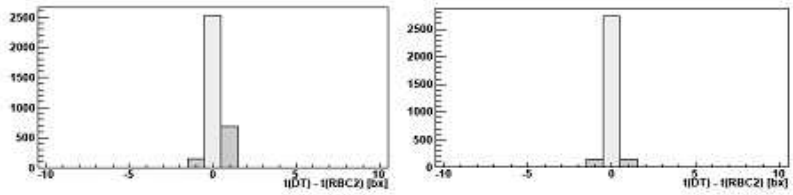

Figure 3: The difference between the two reception times before and after the correction is shown respectively in (a) and (b). Only the events where both systems produced the trigger are included.

The DT local reconstruction allows the determination of segments in the 3D space obtained by analyzing hits in each of the three super-layers, comprised in the DT chambers [2], in the first three stations. Unbiased predictions of the hit positions of cosmic muons on the RPC system are obtained by extrapolating linearly the DT track segments to the nearest RPC chambers. This information is used to determine the detailed local performance of the chambers. The residuals of the reconstructed hit position in the RPC to the track segment extrapolated point is shown in Fig. 4. The width of the residuals is $\sigma = 1.02$ cm, compatible with the expected space resolution of 1.01 cm.

Both the synchronization and the local reconstruction show the excellent correlation of the responses of the two muon systems.

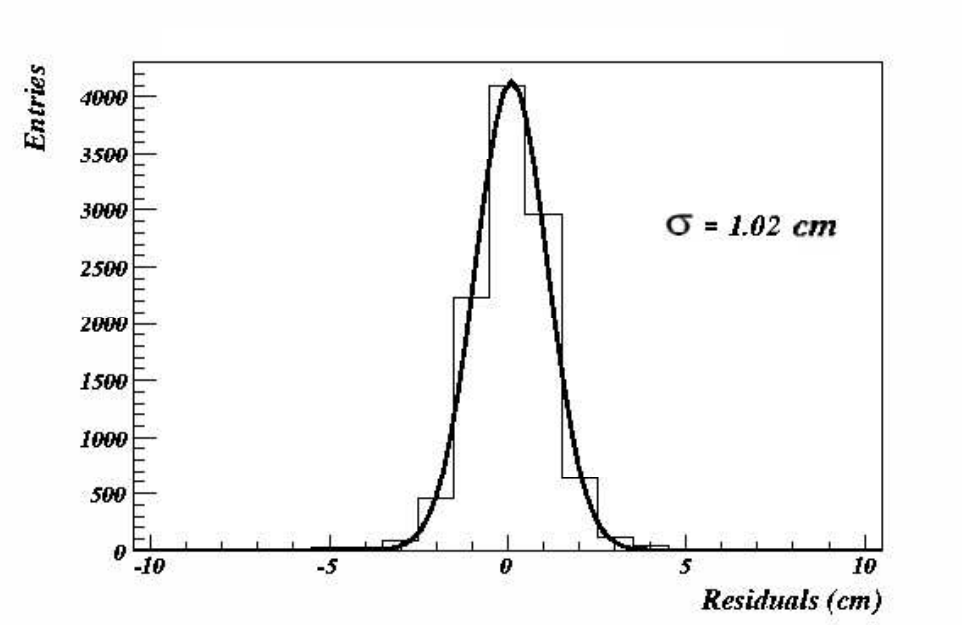

Figure 4: Distribution of residuals between the extrapolated track impact point and the center of cluster on one representive chamber.

4 Noise studies

The use of RPC as trigger detector requires a low noise level to allow the proper functioning of the algorithm and to limit the number of fake triggers. Noise hits can cause fake triggers promoting low transverse momentum muon to high momentum [12]. The measurement of the performance of the chambers is also affected by the noise. It is therefore crucial to determine the noise of the detectors in working running conditions.

Noise rates have been measured under different conditions and with dedicate short periods, by an online procedure, before each data taking, and by a dedicated offine data analysis methods. In the online procedure strips with a rate larger then 10 Hz/cm^2 are masked during the data taking and are therefore excluded in all presented results.

4.1 Online analysis

The noise rates are evaluated from calibration procedures taken at the beginning of each data taking run. The strip signals were counted by the dedicated multi-channel counter modules implemented in the LBs [10].

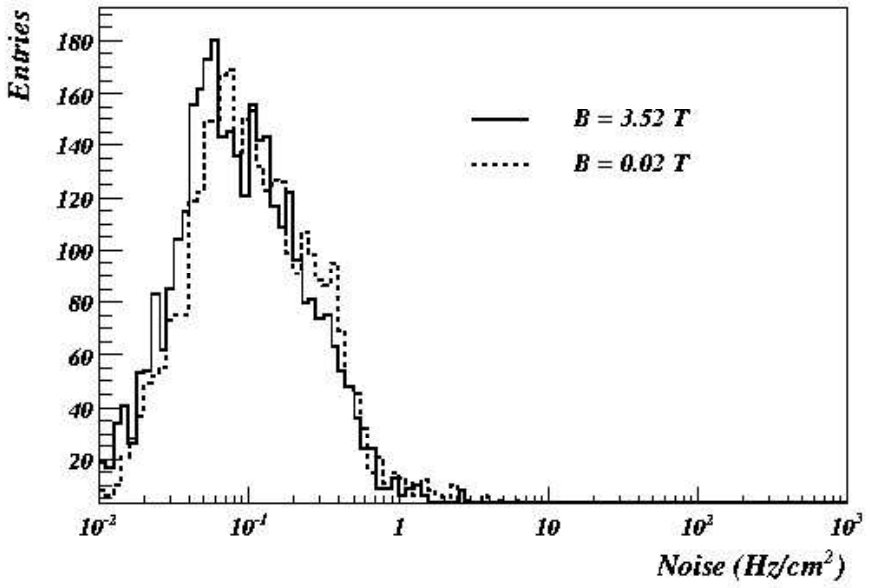

Figure 5: Overall noise distributions for two magnetic field values. All chambers under test are considered.

Noise profiles and history summary plots for each chamber were continuously produced during the entire period of data taking. The number of dead channels was 0.2% and the number of strips exceeding the noise rate of 10 Hz/cm^2 was 1.2%. Most of the masked strips were due to faulty front-end boards which required maintenance. In Fig. 5 the overall noise distribution for all the chambers under test is plotted for different values of the magnetic field. No significant dependence on the magnetic field was observed.

In Fig. 6 a history plot of the average noise over the entire data taking period is shown for some representative chambers. The system was stable in all the possible configuration it was run. The measurement of average noise for the entire system under test is shown in Fig. 7, where, for each eta-partition, the rate was determined over the entire running period. The spread of all measurements is also represented with a bar. The detailed strip profile of one eta-partition affected by relatively larger noise, is presented in Fig. 8. The higher rate, in this case is due to a single strip just below the masking threshold.

4.2 Offline Noise analysis

An independent evaluation of the noise rate was performed by selecting events triggered by the DT system. In each event only sectors where, no DT segments are found and to which the DT segments of the other sector do not extrapolate to any RPC chamber, were considered. This procedure is designed to select regions far from the muon track. A visual scan of several events was also performed to check the reliability of the method. The noise rate is determined by the number of observed reconstructed hits divided by the total acquisition time that is given by the

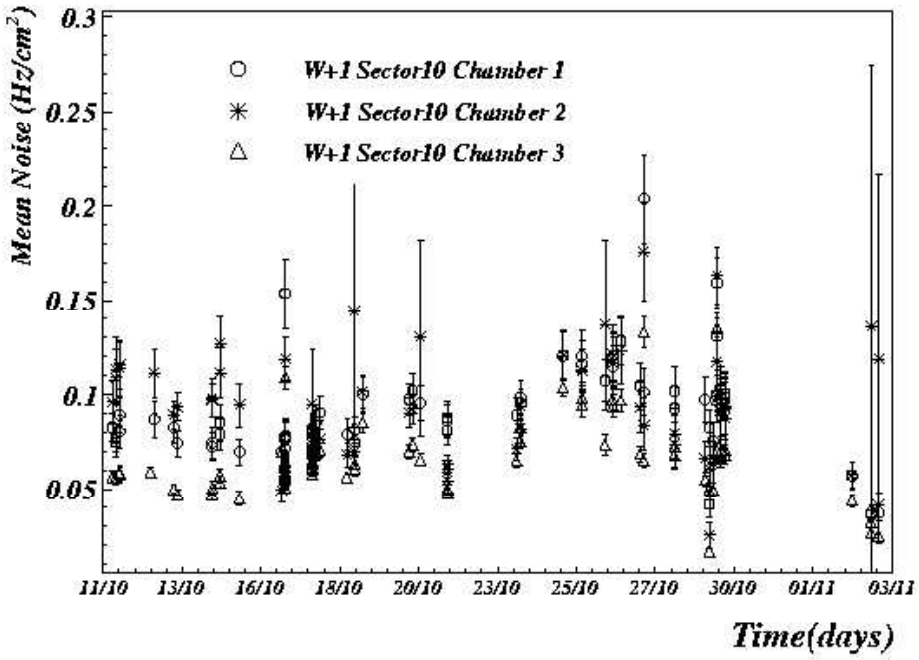

Figure 6: Average noise time chart for few chambers.

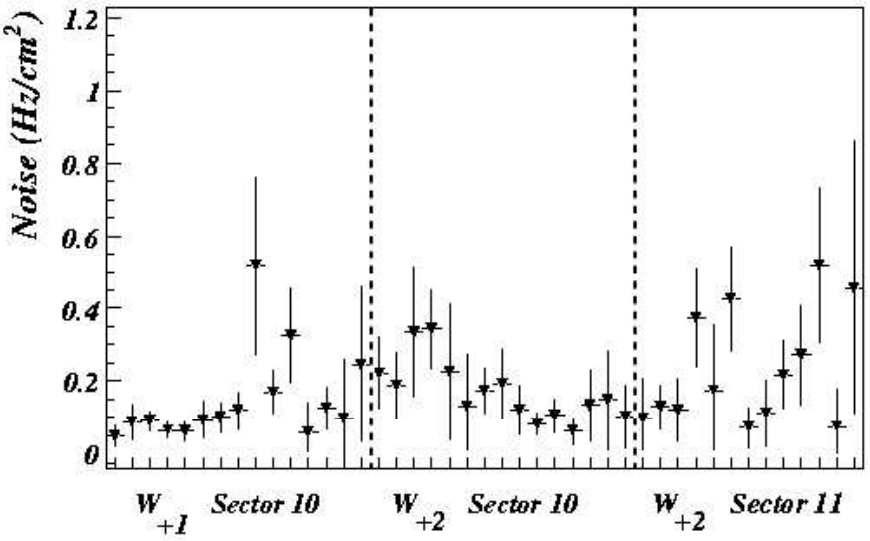

Figure 7: Profile histogram of the noise distribution for the system in operation. Each bin of the distribution corresponds to an eta-partition. The average, represented by full triangle, and the spread, represented by the bars, are calculated with several measurents taken over the entire running period.

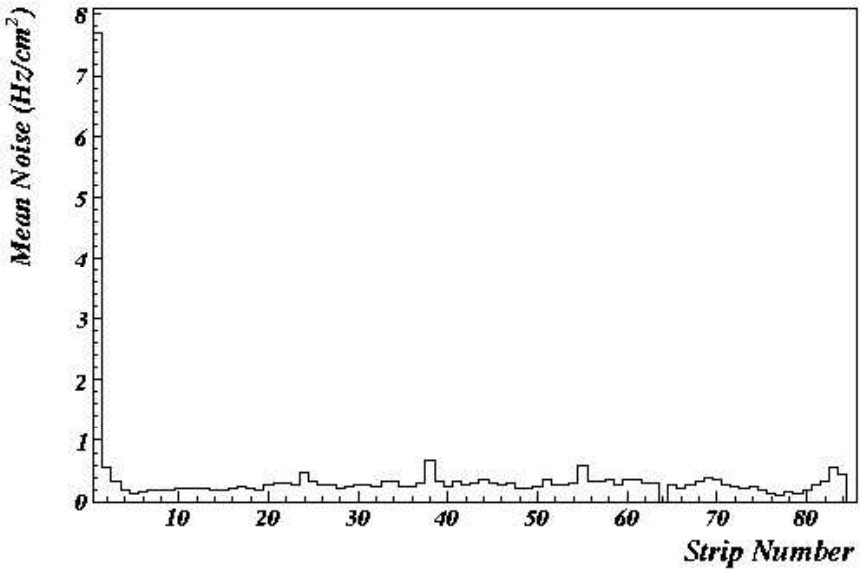

Figure 8: Average noise strip profile for one eta-partion of (bin ♯9 of the previous distribution).

	Noise (Hz/cm^2)
W_{+2} Sect.10	0.11 ± 0.02
W_{+2} Sect.11	0.44 ± 0.06
W_{+1} Sect.10	0.34 ± 0.05

Table 1: Average noise values of all three sectors under test.

number of events and the number of BX read-out. A typical noisy strip multiplicity distribution is given in Fig. 9 that shows the result obtained for Sector 10 of W_{+1}. No events were found with a strip multiplicity exceeding 20 strips fired.

Using this method, the average noise values of the three sectors under test were computed. The average results of the entire running period are given in Table 4.2.

The global results reported in this section, together with the results already discussed for the on-line method in Section 4.1, confirm the extremely low level of noise of the RPC system, well below the CMS requirements of 10 Hz/cm^2.

5 Efficiency studies

The muon trigger efficiency together with the muon reconstruction and identification efficiency are predictable once the chamber efficiencies are determined with high precision.

Efficiencies are measured in small local region using the DT track segments extrapolation already discussed in Section 3, with the additional requirement that in the DT chambers one and only one segment is reconstructed to reject multi-muon events like the one in Fig. 10 or other effects preventing an unambiguous prediction. Event by event, the chamber is considered efficient if a strip is fired exactly in the same eta-partition where the hit was predicted, and in a fiducial region defined by ± 2 strips around the predicted strip. In Fig. 11 the local efficiency for one chamber of sector 10 of W_{+2} is reported for different values of the effective operating voltage.

The global efficiency is then evaluated as average of the local strip by strip efficiency. The efficiency plateau curves for some rappresentative chambers are shown in Fig. 12.

Possible systematic errors to the results, coming from the hit association criteria used for the analysis, are studied. In Fig. 13 the efficiency at $HV_{eff} = 9.2$ kV is given as a function of the dimension of the fiducial acceptance region expressed in number of strips. Values are normalized to the efficiency obtained for ± 5 strips. The figure

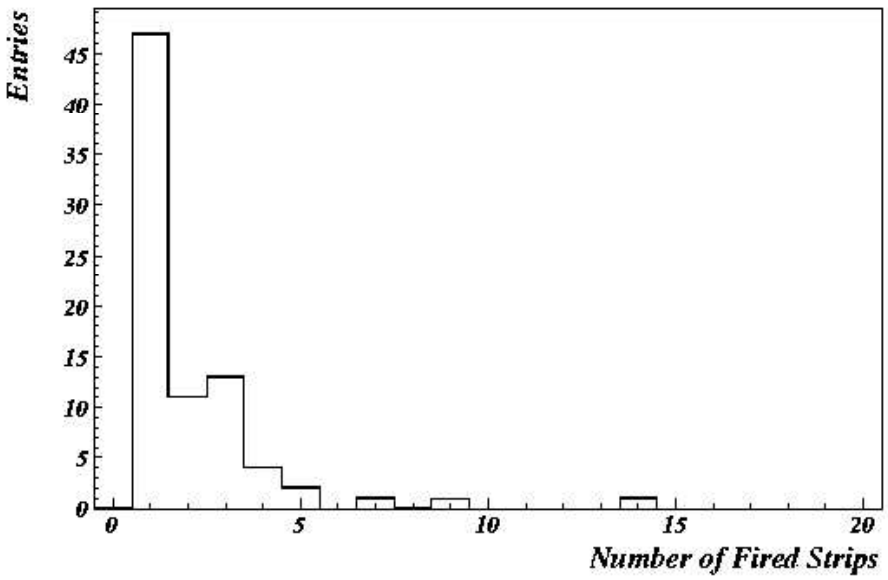

Figure 9: Noisy strip multiplicity distribution for Sector 10 of W_{+1}

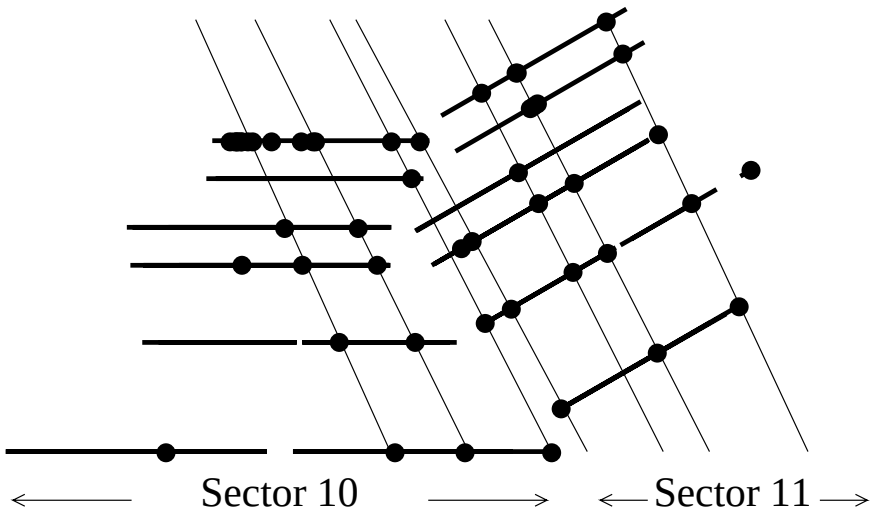

Figure 10: Event display of a multi-muon cosmic event. Superimposed the result of a RPC stand-alone reconstruction.

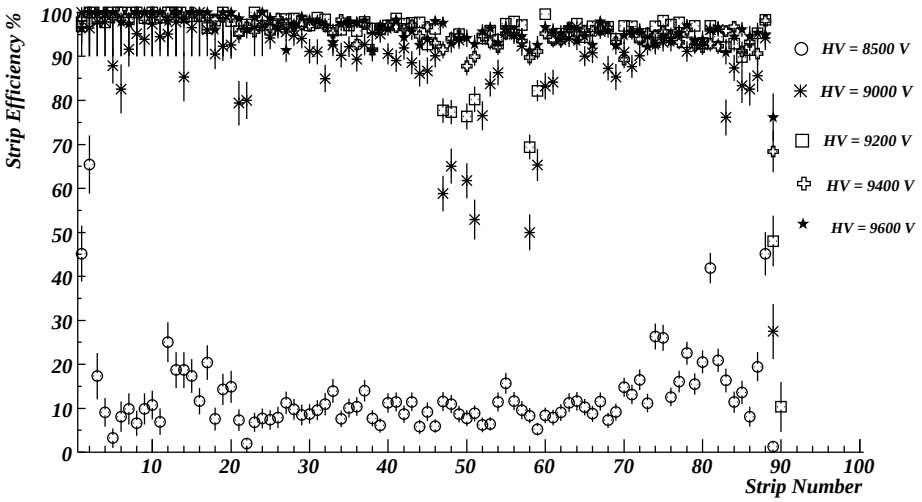

Figure 11: Local efficiency computed along each strip for one chamber of Sector 10 of W_{+2} for different values of the nominal HV.

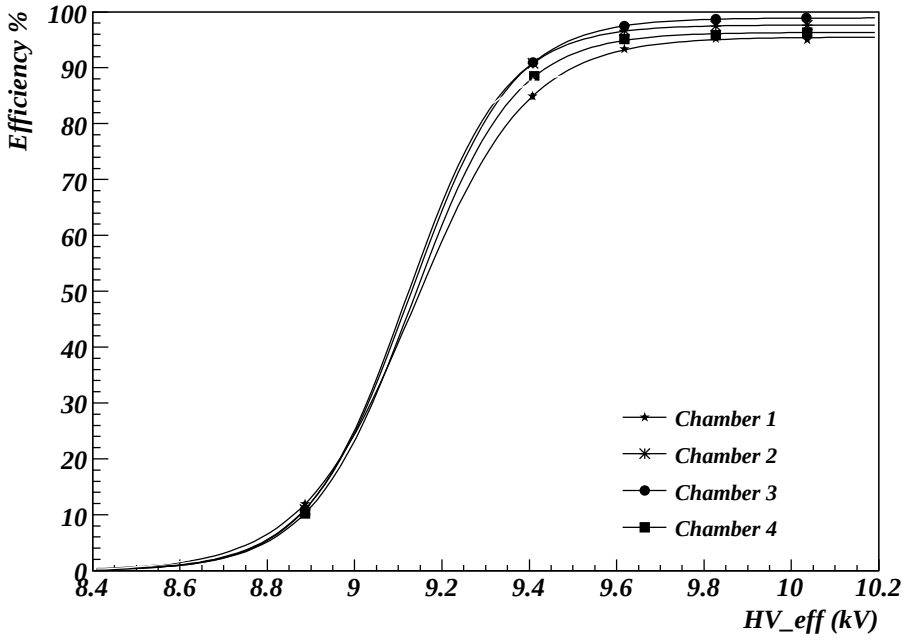

Figure 12: Efficiency plateau for some representive chambers.

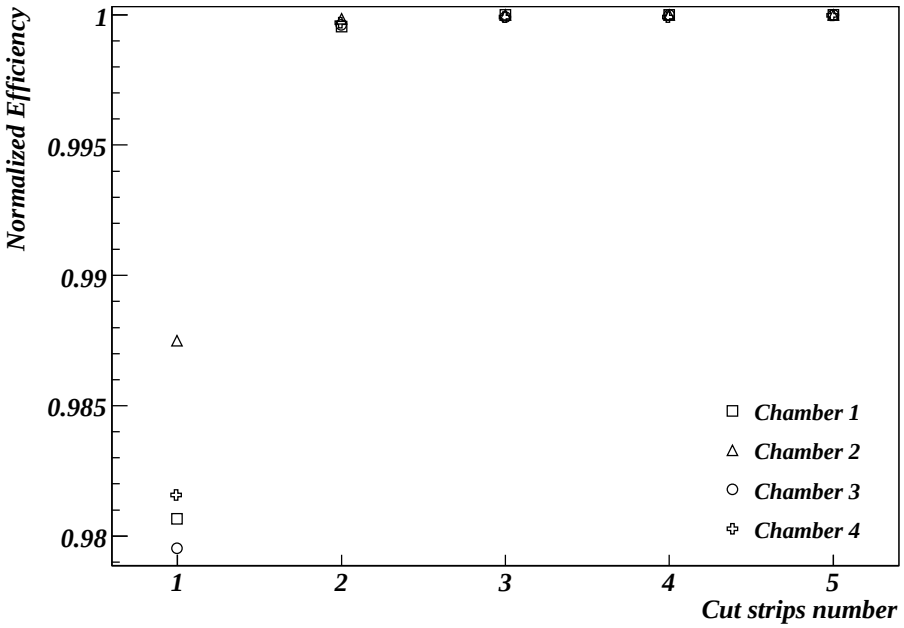

Figure 13: Efficiency as function of the hit acceptance fiducial region. Values are normalized to the efficiency obtained with a $\pm$ 5 strips acceptance region.

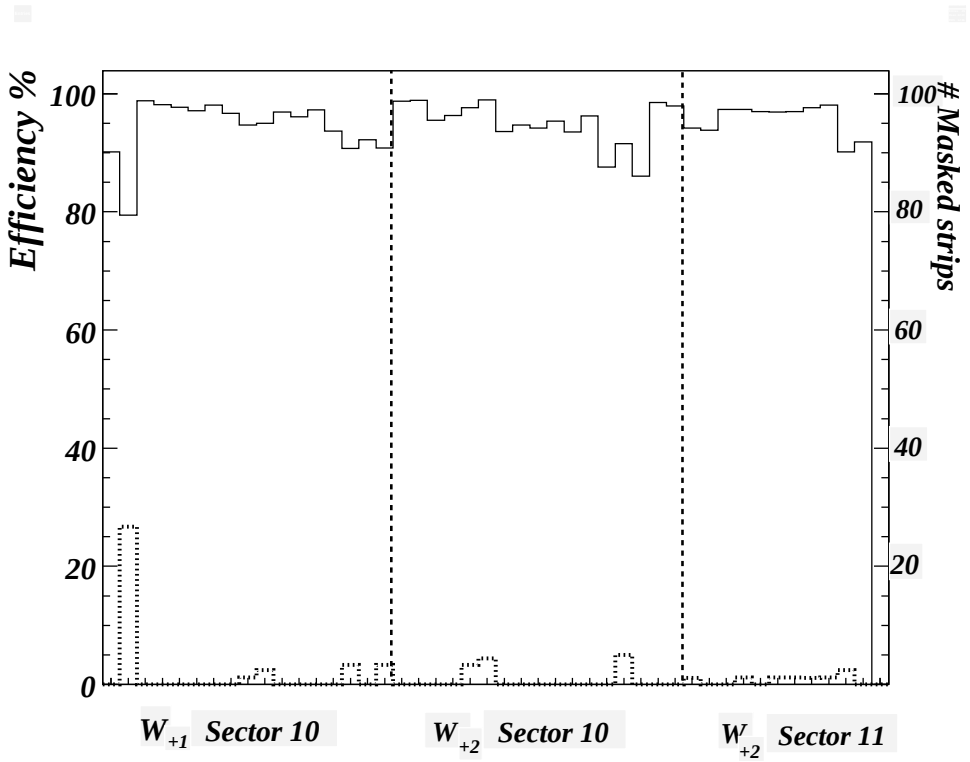

Figure 14: Distribution of the plateau efficiencies for all the chambers in operation. Superimposed (dotted line) is the number of masked strip per chamber.

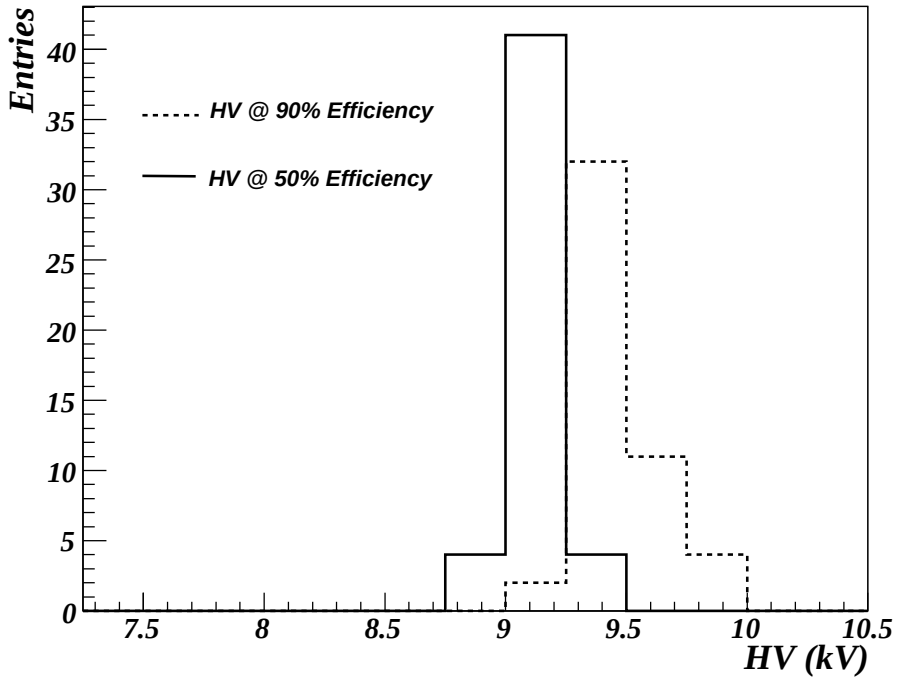

Figure 15: Effective HV distribution at 50%, full line, and 90%, dashed line, of the maximum efficiency.

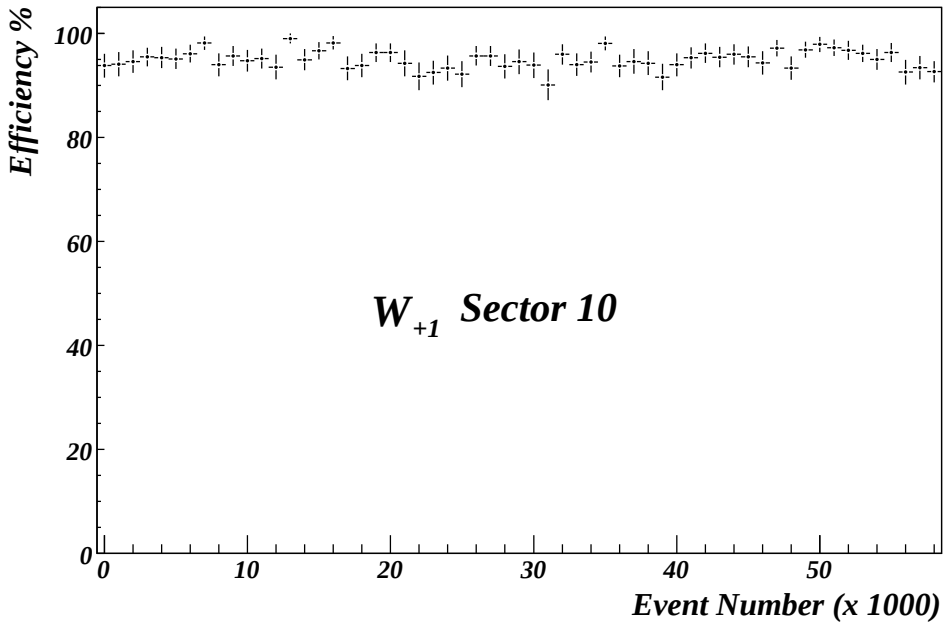

Figure 16: Average efficiency of Sector 10 in W_{+1} computed every thousand event in a typical run.

shows that a fiducial region of ± 2 strips does not introduce any significant bias within the statistics used.

The plateau efficiencies are given in Fig. 14, where each bin corresponds to a given eta-partition. In addition, the number of masked strips in the same eta-partition is superimposed. The lower efficiency for few cases is consistent with the presence of masked strips.

Fig. 15 shows the distribution of the effective HV for each different eta-partition when chambers are operated at 50% and 90% maximum efficiency. The small spread denotes a good homogeneity of the RPC behaviour.

Finally in Fig. 16 is reported the average efficiency for Sector 10 of W_{+1} computed every thousand events that demonstrates the stability of the apparatus during a long run.

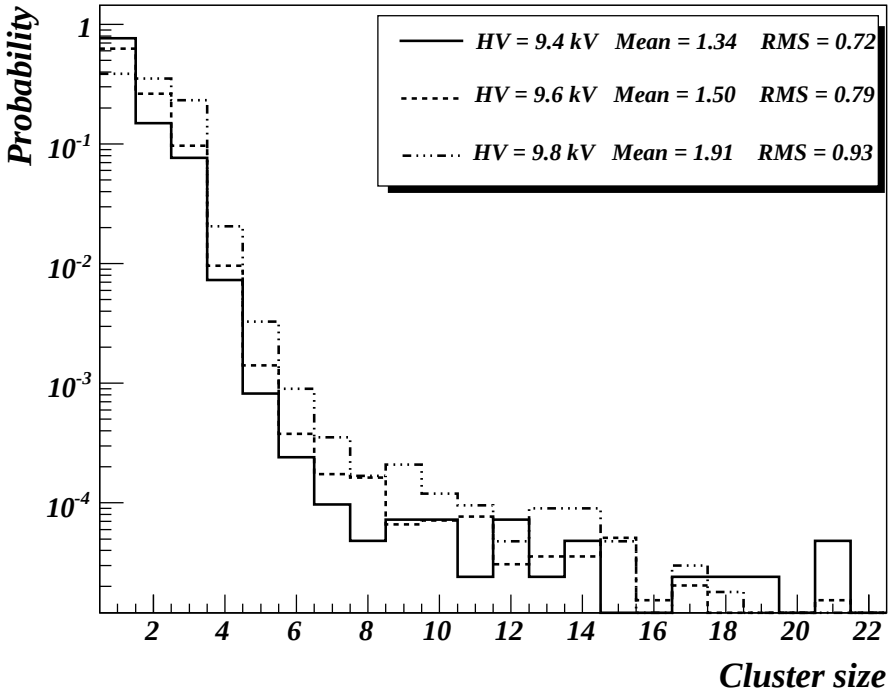

Figure 17: Cluster size distributions at different nominal HV.

6 Cluster size studies

The RPC trigger performance depends strongly on the hit cluster size, defined as the number of adjacent fired strips. A large cluster size could introduce uncertainty in the muon pattern recognition algorithm and originate a significant number of ghost events. The cluster size distributions at different effective high voltages are presented in Fig. 17. The maximum cluster size found was 21.

The cluster size is also studied as a function of the track impact position. The strip corresponding to the extrapolated DT segment is divided into five slices. The average cluster size is then computed for all events for each particular slice. The result is reported in Fig 18. Average cluster size is minimal for track crossing the center of the strip, while it increases if muon hits the edges. This is confirmed by results reported in Fig. 19, where the expected impact point distributions for clusters of different sizes are shown. The strip width has also an impact on the cluster size. In Fig. 20 the average cluster size as function of the layer is given. A slight increase can be noted from outer to inner stations due to the width of the strips.

7 Conclusion

About 5% of the Barrel RPC Trigger system was operated in a CMS data taking period of cosmic measurements. The system behaved steadily with excellent performance with and without magnetic field. The average noise was

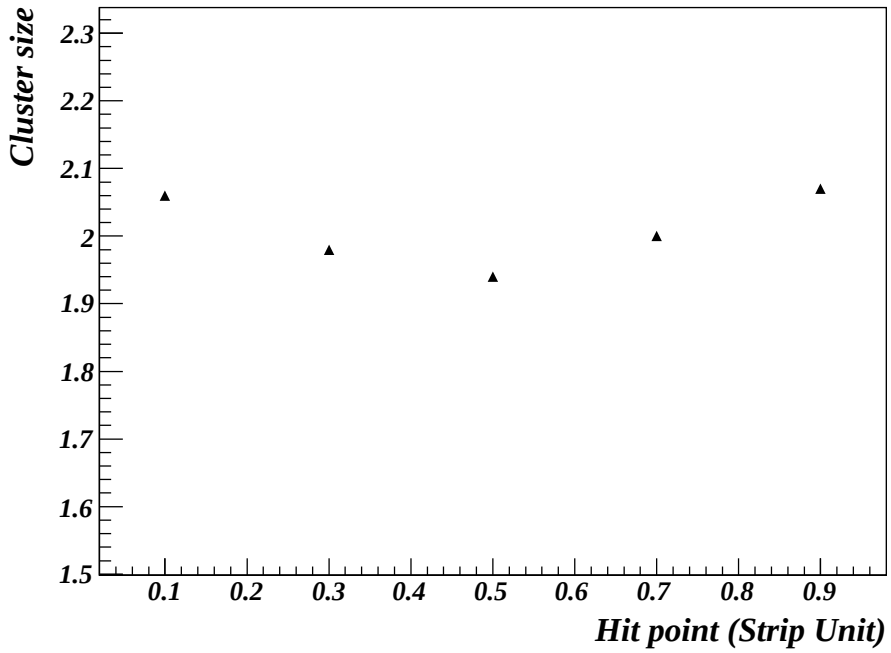

Figure 18: Average cluster size versus the impact point on the strip. The center of the slide is considered as reference.

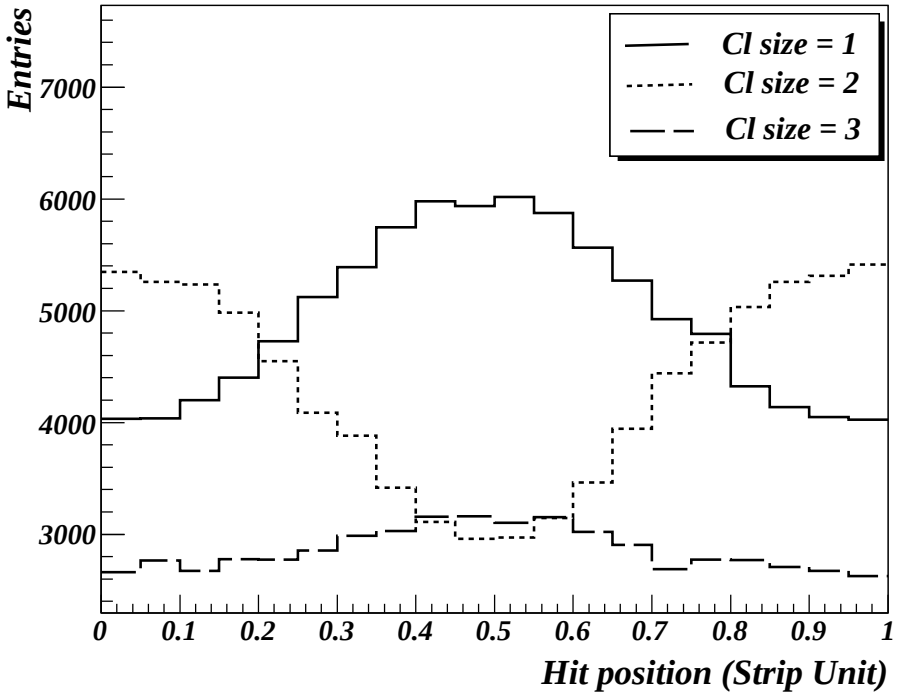

Figure 19: Impact point distribution in strip unit for clusters of different size.

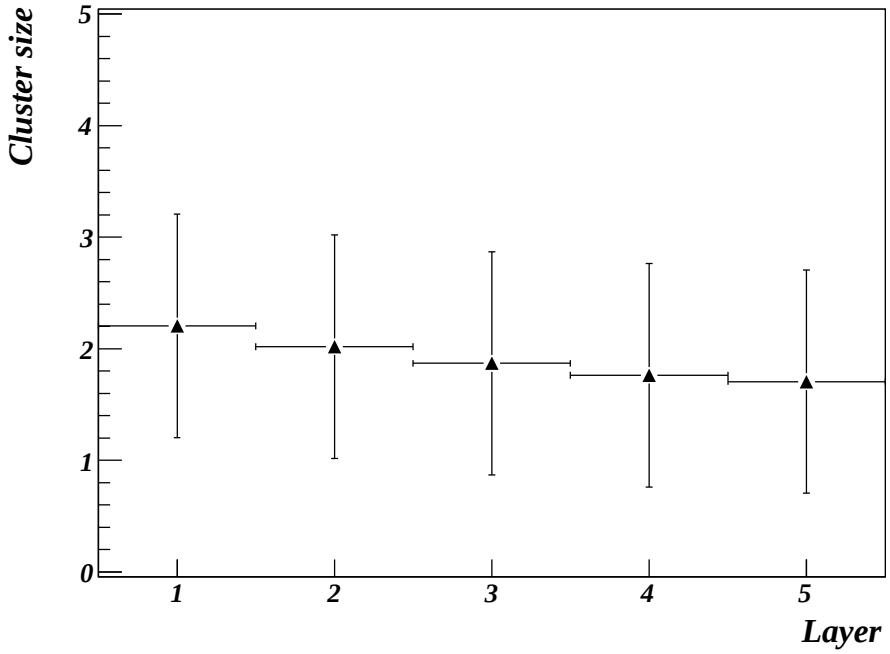

Figure 20: Average cluster size as a function of the RPC layer.

well below 1 Hz/cm^2. All chambers have shown an efficiency greater than 90%. The average cluster size was below 2.

8 Acknowledgement

We would like to thank all RPC CMS technical and engineering collaborators whose valuable contribution made all this happen. A special thank goes to our colleagues of the other sub-detector groups for the very collaborative atmosphere. This work was partially supported by ALFA-EC funds in the framework of the HELEN Program.

References

[1] CMS Collaboration, Technical Proposal, CERN/LHCC 94-38, 1994.

[2] CMS Collaboration, *CMS MUON Technical Design Report*, CERN/LHCC 97-32, 1997.

[3] CMS Collaboration, *The Level-1 Trigger TDR*, CERN/LHCC 2000-038, 2000.

[4] CMS Collaboration, CMS Note *The CMS Magnet Test and Cosmic Challenge (MTCC Phase I and II) Operational Experience and Lessons Learnt*, 2007/05, 2007.

[5] CMS Collaboration, *The CMS experiment at the CERN LHC*, 2008 J. Inst. 3 S08004 (2008).

[6] M. Abbrescia et al., *Resistive plate chambers performances at cosmic rays fluxes*, Nucl. Instrum. Meth. A 359 (1995) 603.

[7] M. Abbrescia et al., *New developments on front-end electronics for the CMS resistive plate chambers*, Nucl. Instrum. Meth. A 456 (2000) 143.

[8] K. Bunkowski et al. *Pattern Comparator trigger algorithm implementation in FPGA*, Proc. SPIE 5125, 165-174.

[9] M. Abbrescia et al., *An RPC-based Technical Trigger for the CMS experiment*, Proceedings of the 12 Workshop on Electronics for LHC and Future Experiments, Valentia, Spain, 25 Sept. 2006.

[10] K. Bukowski et al., *Diagnostic Tools for the RPC Muon Trigger of the CMS Detector Design and Test Beam Results*, IEEE Trans. on Nucl. Science, vol. 52, no. 6, pp. 3216-3222, (2005).

[11] K. Bunkowski et al. *Synchronization methods for the PAC RPC trigger system in the CMS experiment*, Meas. Sci. Technol. 18 (2007) 2446-2455.

[12] S. Altieri et al. *Results from a complete simulation study of the RPC based muon trigger system for the CMS experiment*, Nucl. Instrum. Meth. A 461 (2001) 483.

[13] M. Abbrescia et al., *Cosmic ray tests of double-gap resistive plate chambers for the CMS experiment*, Nucl. Instrum. Meth. A 550 (2005) 116.